A correlation of results measured by cyclic voltammogram and impedance spectroscopy in glucose oxidase based biocatalysts

Marcelinus Christwardana, Yongjin Chung[†], and Yongchai Kwon[†]

Graduate School of Energy and Environment, Seoul National University of Science and Technology,
232 Gongneung-ro, Nowon-gu, Seoul 01811, Korea

Abstract–A new biocatalyst consisting of glucose oxidase (GOx) and polyethylenimine (PEI) immobilized on carbon nanotube (CNT) (CNT/PEI/GOx) was developed, while cyclic voltammogram (CV) behaviors of several related catalysts including the CNT/PEI/GOx were analyzed in terms of charge transfer resistances (R_{ct}s) obtained by measuring Nyquist plots using electrochemical impedance spectroscopy (EIS). A qualitative correlation between the flavin adenine dinucleotide (FAD) redox reactivity measured by the CV and R_{ct} was established. As factors affecting both the FAD reactivity and R_{ct}, concentrations of GOx, glucose, and phosphate buffer solution, electrolyte pH and ambient condition were considered and evaluations of the catalysts using the CV curves and Nyquist plots confirmed that a pattern in the FAD reactivity was closely linked to that in the R_{ct}, implying that FAD reactivities of the catalysts are predicted by the measurements of their R_{ct}s. Even regarding performance of the enzymatic biofeul cells (EBCs) using the reacted catalysts, a pattern of the R_{ct}s is compatible with that in the maximum power densities (MPDs) of the EBCs.

Keywords: Glucose Oxidase, Charge Transfer Resistance, Flavin Adenine Dinucleotide Redox Reactivity, Enzymatic Biofuel Cell, Cyclic Voltammogram

INTRODUCTION

The utilization of glucose oxidase (GOx) as a catalyst for the enzymatic biofuel cell (EBC) and glucose biosensor is very promising [1-3] compared other types of enzymes [4,5]. Since the EBC and glucose biosensor using the GOx-based catalysts consider glucose as a fuel in the blood circulation system of human body, they can be used for implantable bioelectrical devices [6]. To date there have been many attempts to develop the EBC and glucose biosensor using the GOx-based catalyst, but due to its limitations, such as poor catalytic activity, low enzyme loading, sluggish charge transfer rate and short lifetime, the progress for development of such bioelectrical devices has been slow [7-10].

To address these problems, support materials like the carbon nanotubes (CNT) and graphene have been often suggested because it is known that they could promote the immobilization of enzyme moieties [11,12]. For instance, non-covalent adsorption [13], encapsulation [14], covalent coupling [15], affinity bonding [16] and enzyme cross-linking [17] methods have been the GOx immobilization methods suggested. Of these, the GOx immobilization via covalent coupling and adoption of the enzyme catalytic structure to the EBC and glucose biosensor have been widely tried because of their easy fabrication process. Based on that, enhancements in the performance of bioelectrical devices, such as high maximum power density (MPD) and sensitivity, can be achieved [18-20]. Furthermore, with these methods, GOx molecules could be strongly

immobilized and promote the glucose oxidation reaction (GOR) that is a required reaction to operate the EBC and glucose biosensor effectively.

For fabricating excellent catalytic structure, it is critical to choose superior entrapping polymer (EP) that should be positively charged because the support material and GOx are all negatively charged and play a bridging role with both the support material and GOx [21]. In this regard, polyethylenimine (PEI) is one of the proper EPs, which is positively charged in neutral pH (isoelectric point; pI: ~10.5) [22]. Due to such polarity, the support material and GOx are easily entrapped with the PEI by an attractive force [23]. PEI also has abundant amine functional bonds, and then the bonds are closely attached to the amine bonds of GOx to form a strong physical bonding. As a result, PEI is probably acting as a highway for promoting electron transfer from the active sites (flavin adenine dinucleotide (FAD)) that are located deep inside GOx via the supporter material to the electrode [24].

According to Shervedani et al., most bioelectrical devices consist of two main parts connected in series: biochemical recognition system and transducer [25]. The role of the biochemical recognition system is to translate information produced from the biochemical domain to the output signal, while that of transducer is to transfer the output signal to the electrical domain. Based on that, the glucose based bioelectrical transducers are usually dependent on potentiometric or amperometric detection [26,27]. Here, the conventional potentiometric or amperometric detection relies on potential or current, respectively, that was obtained from oxidation reaction of glucose to gluconolactone by the catalytic activity of GOx. However, the detections have fundamental limitations, such as the noisy response and gradual decadence [26]. To alleviate such

[†]To whom correspondence should be addressed.
E-mail: kwony@seoultech.ac.kr, yjchung@seoultech.ac.kr

difficulties, a Nyquist plot of electrochemical impedance spectroscopy (EIS) is considered because the EIS can produce smoother response, powerful, nondestructive, and more informative than amperometric or potentiometric detection [25].

In this study, we investigated the electrochemical correlation between the Nyquist plots using EIS and cyclic voltammogram (CV) behavior of CNT/PEI/GOx structure. Here, PEI is considered EP, while CNT as supporter material. Also, the CNT/PEI/GOx structure is fabricated by the layer by layer (LbL) method between PEI and GOx [22]. To confirm viability of the CNT/PEI/GOx structure as well as validity of the electrochemical correlation, performance of the EBC using CNT/PEI/GOx was also evaluated.

EXPERIMENTAL

1. Materials

The multiwall carbon nanotubes (MWCNT, average diameter 20 nm, purity is higher than 99%) were obtained from Carbon NanoTech MR99 (Gyeongbuk, Korea). Glucose oxidase (GOx, from *Aspergillus niger* type X-S, 150.000 U·g^{-1} solid) and polyethylenimine were purchased from Sigma Aldrich (Milwaukee, WI, USA).

2. Preparation of CNT/PEI/GOx

CNT/PEI/GOx layers were prepared by the layer-by-layer (LbL) deposition between PEI on MWCNT and GOx as shown in Fig 1(a). First, 10 mL of 2.5 mg·mL^{-1} PEI solution (in 0.01 M PBS pH 7.4) and 50 mg of CNT were mixed. The CNT/PEI mixture solution was sonicated for 10 min and stirred for 2 h. Then, the mixture was centrifuged. Deionized (DI) water was used to remove excessive PEIs by washing method. After that, the mixture was immersed into the different concentrations of GOx solution (2, 4, 6, 8 and 10 mg·mL^{-1}) overnight and the different mixtures including GOx were centrifuged again and their supernatants were removed, completing the GOx/PEI/CNT catalyst [10,22,28].

3. Half-cell and Full-cell Electrochemical Characterization

The electrochemical measurements involved using a computer connected potentiostat (SP-240, BioLogic). A pt wire and Ag/AgCl (soaked in 3.0 M NaCl) were used as the counter and reference electrodes for three electrode cell measurements. To fabricate the working electrode, 10 μL of catalytic ink was dropped on the glass carbon electrodes (GCE) and dried. Then, 5 wt% Nafion solutions were dropped on the catalytic ink-loaded GCE [29,30]. PBS was used as an electrolyte to promote redox reaction of the active sites within GOx, while high purity N$_2$ and air gases were provided to the electrolyte to create anaerobic (N$_2$ state) and aerobic (air state) conditions.

The impedance spectra were determined in the frequencies from 60 kHz to 10 Hz with ten steps per decade, while the modulating potential was 10 mV. All the Nyquist plots were determined with approach by Randles equation, as shown in Fig. 1(b). In the circuit formed by the Randles equation, R$_s$ and R$_{ct}$ stand for the solution resistant and charge transfer resistant, while C$_{dl}$ and Z$_w$ stand for the double layer capacitance and Warburg diffusion region.

To measure the polarization curves from the EBC single cells, a potentiostat was also connected with a frequency response analyzer (FRA). By coupling the FRA with the potentiostat, the power output was analyzed as a product of current and potential. Pt/C was used as cathode catalyst. For cathode, 100 cc min^{-1} O$_2$ gas was fed to the electrode, while 0.2 M glucose solution was circulated as a fuel for the anode electrode. During the EIS measurement, H$_2$ gas was fed into the cathode to consider only electron transfer resistance occurring in the anode.

RESULTS AND DISCUSSION

1. Optical Characterization of CNT/PEI/GOx

Morphology of the catalyst was investigated using scanning electron microscope (SEM). The SEM images are represented in Figs. 2(a)-(b). According to the images, an average diameter of bare CNT was ~20 nm (Fig. 2(a)), while that of CNT/PEI/GOx was ~24 nm (Fig. 2(b)). Even by visual inspection, the CNT bundles of Fig. 2(b) seem to be thicker than those of Fig. 2(a), meaning that the PEI and GOx moieties were well immobilized on the CNT in Fig. 2(b).

2. Electrochemical Characterization of CNT/PEI/GOx

It is important to explore the PEI adoption effect by measuring active surface area of the catalysts and redox reaction rate of the FADs that were placed deep inside of the GOx. For doing that, the CV curves of GCE, CNT, CNT/PEI, and CNT/PEI/GOx were measured (Fig. 3(a)). About the measurements, there are two important observations. First, there were no redox peaks in the bare GCE, CNT and CNT/PEI, while there was a pair of redox peaks at −0.46 V
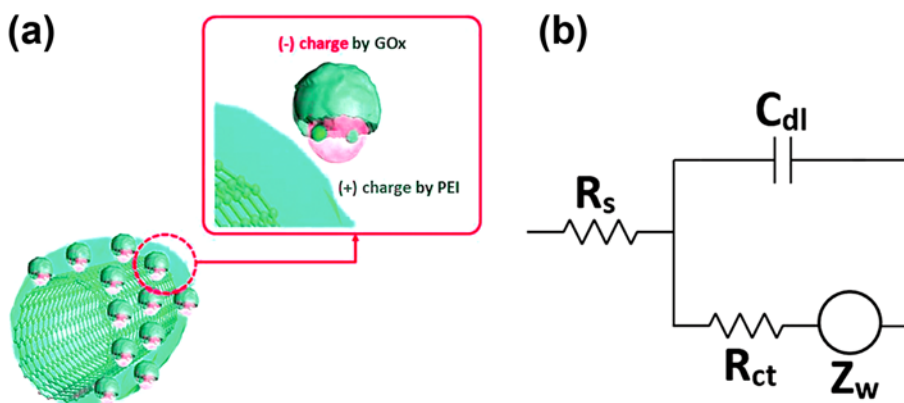

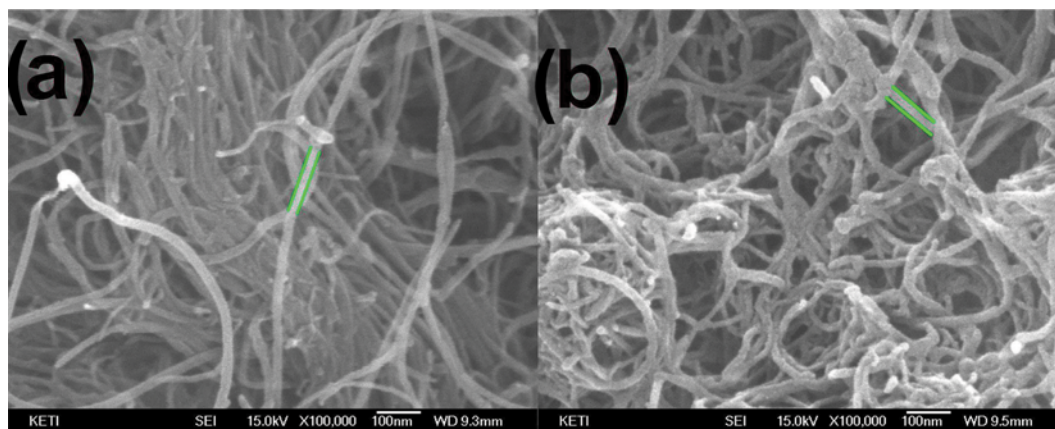**Fig. 1. Schematics of (a) CNT/PEI/GOx catalyst and (b) Randles circuit diagram.**

Fig. 2. SEM images of (a) bare CNT and (b) CNT/PEI/GOx catalysts.
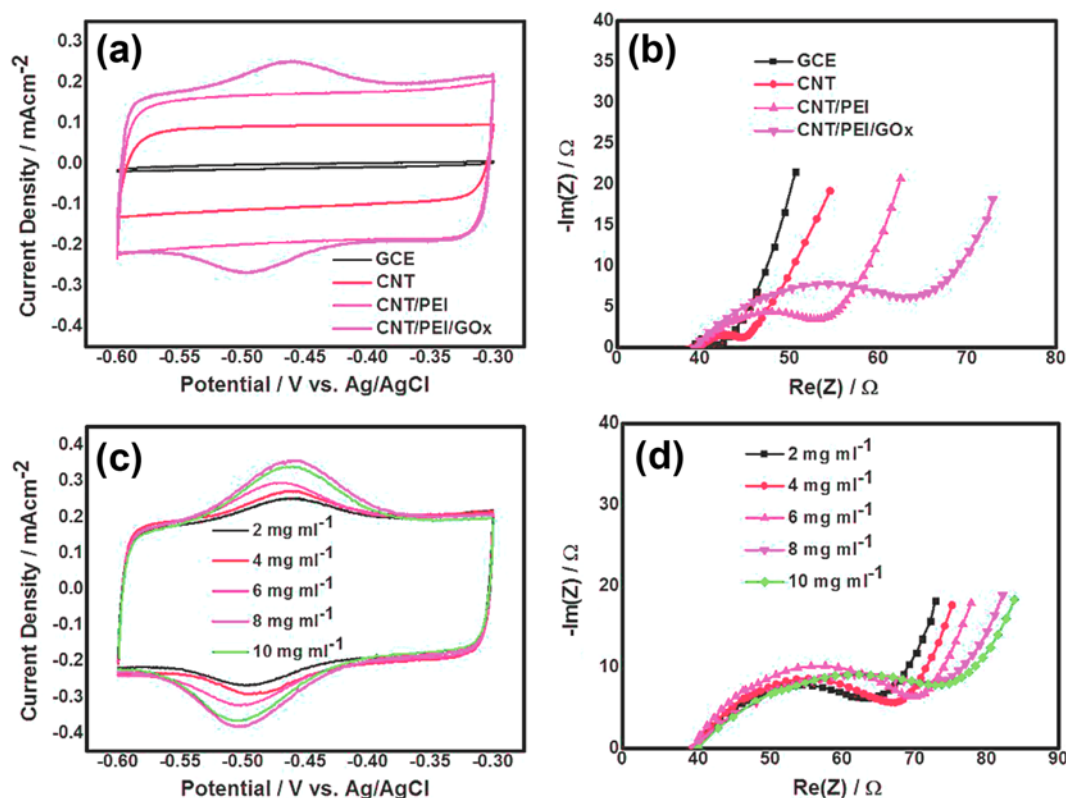

Fig. 3. (a) Cyclic Voltammogram (CV) curves and (b) Nyquist plots of the GCE, CNT, CNT/PEI, CNT/PEI/GOx catalysts and (c) CV curves and (d) Nyquist plots of the CNT/PEI/GOx catalysts measured under GOx concentrations of 2, 4, 6, 8 and 10 mg·mL^{-1}. For the tests, 0.01 M PBS (pH 7.4) acted as electrolyte at N_2 state and potential scan rate was 100 mV·s^{-1}.

vs. Ag/AgCl in the CNT/PEI/GOx. The redox peak is attributed to the FAD redox reaction ($GOx(FAD)+2H^++2e^- \leftrightarrow GOx(FADH_2)$), and second, in a comparison of the bare CNT and CNT/PEI, a background current of the CNT/PEI increased. It was due to adoption of the PEI. Such adopted PEI, which possesses excellent entrapping ability, modified the property of CNT surface in a more hydrophilic way, thereby both the entrapping capability of PEI and hydrophilic surface made formation of the electrical double layer easy, increasing the background current.

To confirm these phenomena using the EIS, the related Nyquist

plots were measured (Fig. 3(b)). In the Fig. 3(b), R_s was similar in all catalysts (39.3-39.9 Ω), whereas R_{ct} increased with a sequential addition of the CNT, PEI and GOx to the GCE from 3.8 to 11.9 Ω (CNT on the GCE), from 11.9 to 14.8 Ω (CNT/PEI on the GCE), from 14.8 to 28.5 Ω (CNT/PEI/GOx on the GCE), respectively. Since the PEI is EP and relatively nonconductive [31,32], the PEI decreases conductivity of the CNT from ~10^6-10^7 to ~43 S·cm^{-2} [33,34]. Such effect of PEI was already reported [31]. GOx also induces the same result, meaning that use of the GOx would increase R_{ct} due to its nonconductive property [35]. One thing to mention here was War-

burg diffusion region of the CNT/PEI was nearly 45°, which is attributed to the semi-infinite diffusion of protons occurring at the interface between the CNT/PEI and electrolyte [36].

The catalytic activity of the CNT/PEI/GOx was measured to determine an optimal GOx concentration under various GOx concentrations because the optimal concentration leads to the highest redox reaction rate of FAD. It was gained by peak current density of the FAD redox reaction measured by the CV curves (Fig. 3(c)). According to the Fig. 3(c), the FAD redox reaction peak increased until the GOx concentration reached $8 \, mg \cdot mL^{-1}$ and in the GOx concentration of $10 \, mg \cdot mL^{-1}$, the peak was a little dropped, confirming that the optimal concentration of GOx was $8 \, mg \cdot mL^{-1}$ with the current density of $0.37 \, mA \cdot cm^{-2}$. Fig. 3(d) represents the Nyquist plots showing EIS behavior of the CNT/PEI/GOx catalyst measured with the increment in GOx concentration. According to Fig. 3(d), R_s was almost the same in all catalysts (39.45-39.84 Ω), whereas R_{ct} increased from 28.5 to 39.1 Ω during an increment of the GOx concentration from 2 to $10 \, mg \cdot mL^{-1}$. As explained, because the GOx

is non-conductive, it was expected that the R_{ct} would increase with an addition of the GOx concentration and the increase in R_{ct} meant an increment in the amount of immobilized GOx [35]. Also, regarding the optimal GOx concentration, there was a difference between results obtained from CV curves and Nyquist plots (by CV curves, $8 \, mg \cdot mL^{-1}$ was optimal GOx concentration, while by Nyquist plots, $10 \, mg \cdot mL^{-1}$ was optimal one). It is apparent evidence that in GOx of more than $8 \, mg \cdot mL^{-1}$, electron transfer from GOx to electrode was not effective although more GOx moieties were immobilized on the CNT/PEI.

In next, it is also important to understand the effect of the PBS electrolyte concentration on catalytic activity of the CNT/PEI/GOx. For that, FAD redox reaction rate of the CNT/PEI/GOx was measured under three different concentrations of PBS electrolyte solution (Fig. 4(a)). Fig. 4(a) implies two results. First, as the PBS concentration increased from 0.01 to 1 M, the FAD redox reaction peak decreased. It is probably due to an increase in the concentration of ionic charges, such as Na^+, Cl^-, PO_4^{3+} and K^+ that are
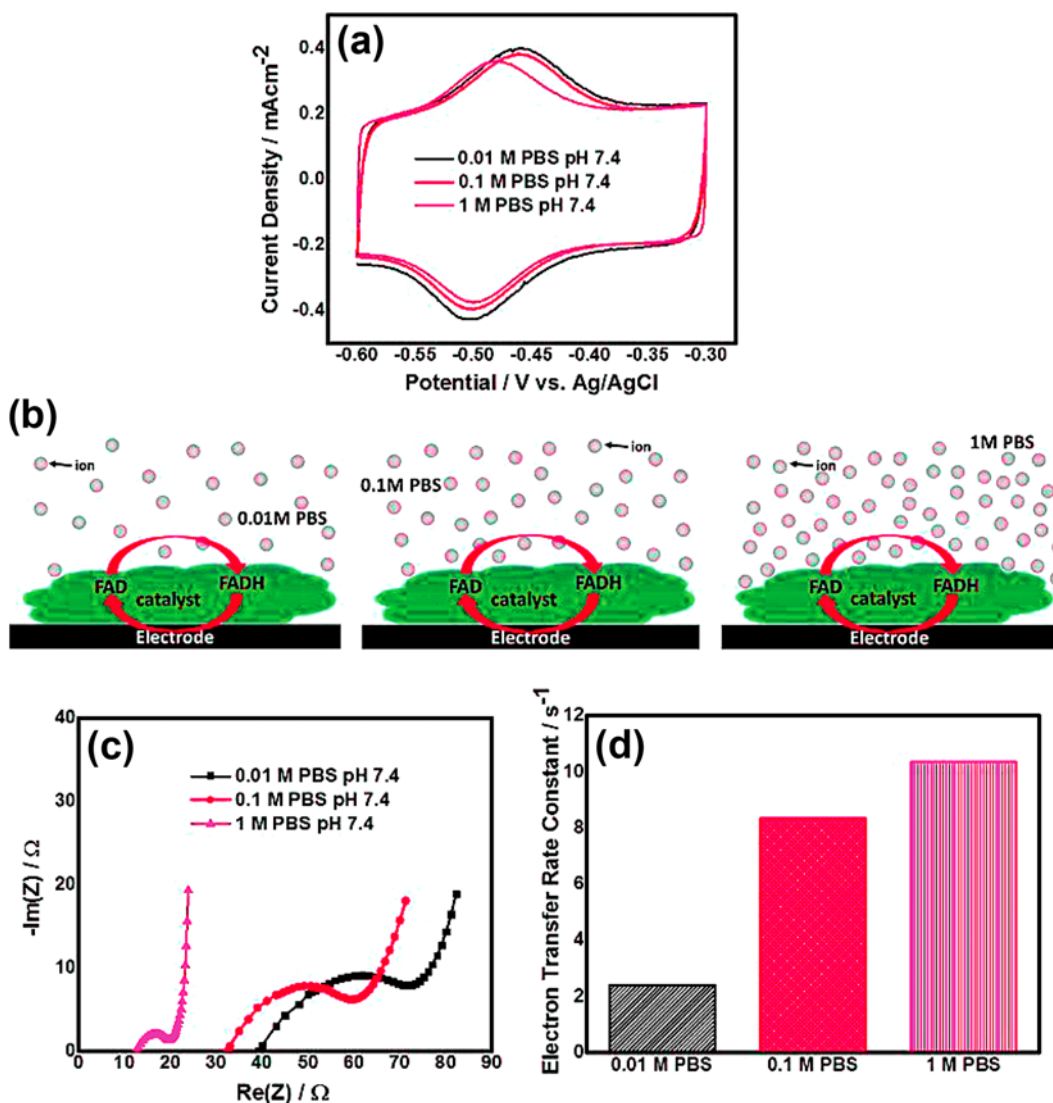

Fig. 4. (a) CV curves and (b) Nyquist plots of the CNT/PEI/GOx catalysts measured under PBS (pH 7.4) concentrations of 0.01, 0.1 and 1 M at N_2 state, while (c) is their electron transfer rate constants.

contained in the PBS solution as forms of NaCl, KCl, NaHPO$_4$ and KH$_2$PO$_4$ [37]. Such increased ionic charges would increase conductivity of the electrolyte and then they would be accumulated at the interface between the electrode (including catalyst) and electrolyte [38], preventing FAD redox reaction in the catalyst surface and having the FAD redox reaction peaks decrease as shown in Fig. 4(b).

Second, anodic current peak of the CNT/PEI/GOx in 1.0 M PBS was slightly shifted to the negative potential direction with a decrease in ΔE_p. The narrower ΔE_p means that the FAD redox reaction caused by the catalyst is controlled by the surface reaction and electron transfer rate of the catalyst is high [39,40]. Fig. 4(c) presents Nyquist plots of the experimental sets measured in the Fig. 4(a). Regarding R_s, the CNT/PEI/GOx catalyst using 0.01 M PBS had the highest R_s (39.7 Ω), while the catalysts using 0.1 and 1 M PBS showed R_ss of 32.4 and 12.9 Ω On the other hand, in a comparison of R_{ct}, the catalyst using 1 M PBS had the highest R_{ct} (8.5 Ω), while the catalyst using 0.1 and 0.01 M PBS showed R_{ct}s of 29.6 and 37.7 Ω

The low R_s and R_{ct} in the catalyst using 1 M PBS are due to a high electrolyte conductivity derived from ionic charge and, because of that, confirm that electrolyte also plays a role in connecting between CNT and GOx (catalyst) like mediator for electron transfer [24]. Especially, low R_{ct} indicates that system is in a highly conductive state (due to high ionic charge), so the electron mobility and its transfer rate constant are high in high conductive system as shown in Fig. 4(d).

It is also important to understand the relationship between the pH of electrolyte and peak potential of the FAD redox reaction (Fig. 5(a)). According to the Fig. 5(a), as the pH of electrolyte increased from 4 to 9, the peak potential of FAD redox reaction linearly dropped with slopes of -59.6 and -60.1 mV·pH^{-1} for the oxidation and reduction reactions. These values were compatible with the reference value (-58.6 mV·pH^{-1}) for desirable two-electron and two-proton reactions [41-43].

Fig. 5(b) presents the Nyquist plots showing EIS behavior of the CNT/PEI/GOx catalyst in different electrolyte pHs (from pH 3 to 9). There are several noticeable results. First, with an increase in the electrolyte pH from pH 7.4 to 9, R_s decreased from 39.9 to 38.3 Ω and R_{ct} decreased from 37.7 to 35.3 Ω. It is attributed to

the ionic charge produced from NaOH (base chemical) included for the pH adjustment. Namely, the NaOH solution is decomposed and then it is divided into OH$^-$ and another proton (Na$^+$) that are probably accumulated in the electrolyte solution. As we explained in previous part, accumulation of the ionic charge induces decreases in the R_s and R_{ct}. Second, in reduction of the pH (from pH 7.4 to 5 and 3), both R_s and R_{ct} decreased (from 39.7 to 17.9 and 9.0 Ω for R_s, and from 37.7 to 17.7 and 15.2 Ω for R_{ct}). Similar to the NaOH effect, the acid chemical (H$_2$SO$_4$) fed for the pH adjustment is decomposed and then it is divided into H$^+$ and another electron (SO$_4^{2-}$) that are probably accumulated in the electrolyte solution, lowering the R_s and R_{ct}. This conductivity-improved electrolyte facilitates electron transfer of the FAD redox reaction inside the GOx [44].

3. Performance of Glucose Biosensor Adopting CNT/PEI/GOx

Fig. 6(a) shows CV curves of the CNT/PEI/GOx catalyst that were operated at aerobic condition with the addition of glucose. As the glucose concentration increased, the CV curve of the CNT/PEI/GOx catalyst was up-shifted. Since the glucose oxidation reaction (GOR) (Glucose→Gluconolactone+2H$^+$+2e$^-$) produced two protons and two electrons, such produced proton and electrons were consumed for the reduction reactions of the FAD and O$_2$ [18]. Fig. 6(b) shows the Nyquist plots of the CNT/PEI/GOx catalyst measured with an increase in glucose concentration from 0 to 10 mM. According to Fig. 6(b), R_{ct} of the CNT/PEI/GOx catalyst decreased from 38.9 to 30.1 Ω, while its R_s was almost the same (39.2-39.8 Ω). The decrease in R_{ct} is due to the GOR that affects the FAD reduction reaction as previously reported [25,45]. As glucose concentration increases, the GOR occurs more often and proton/electron pairs produced by the reaction are then consumed for ORR and FAD redox reaction, indicating that electron transfer between electrolyte and electrode including the enzymatic catalyst is facilitated. With that, conductivity in the electrode also gradually increases and such increased conductivity induces decrease in R_{ct}.

Fig. 6(c) represents the effect of glucose on FAD redox reaction in N$_2$ state. There was no change in CV curve irrespective of glucose provision. It is explained that GOR did not affect the FAD redox reaction significantly, meaning that O$_2$ mediator is needed to bridge electron transfer between the GOR and FAD redox reaction [24]. For that reason, both R_s and R_{ct} did not change very much
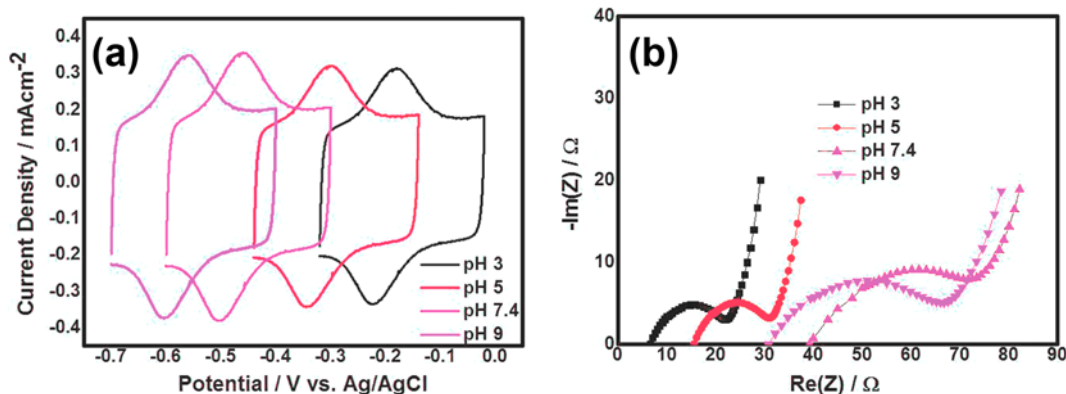

Fig. 5. (a) CV curves and (b) Nyquist plots of the CNT/PEI/GOx catalysts measured under electrolyte pHs of 3, 5, 7.4 and 9. For the tests, 0.01 M PBS (pH 7.4) was used as electrolyte at N$_2$ state and potential scan rate was 100 mV·s^{-1}.
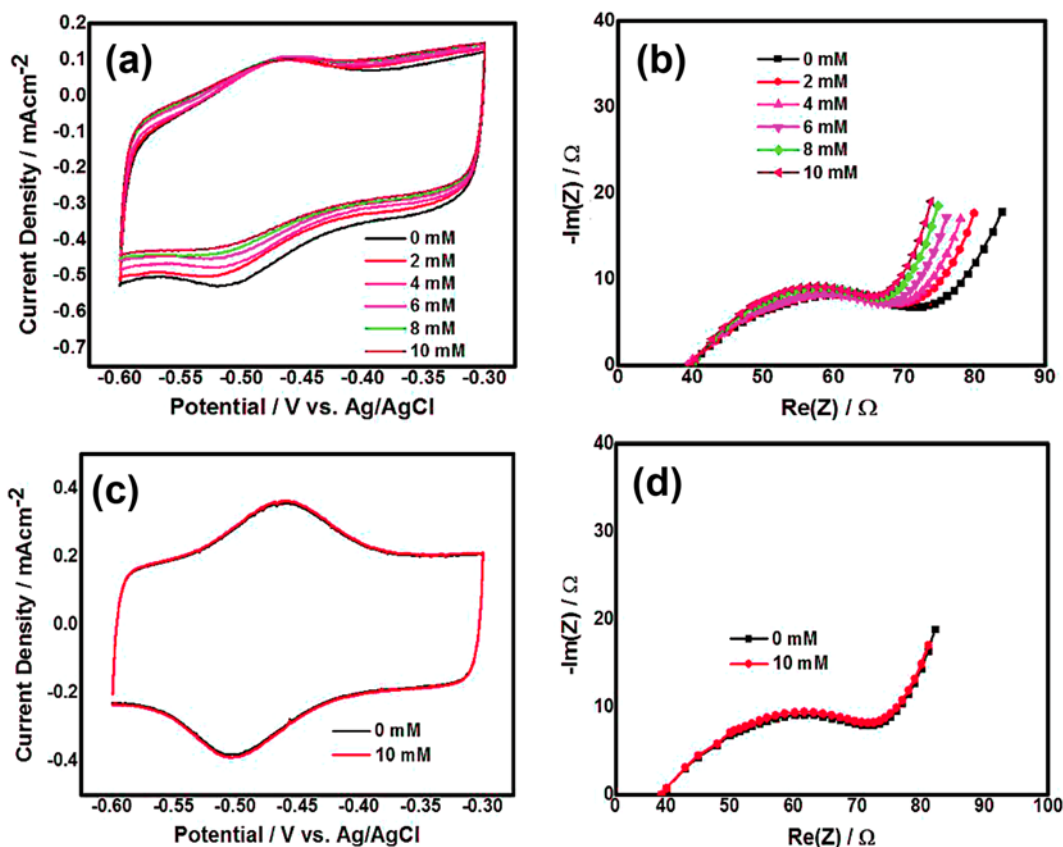
Fig. 6. (a) CV curves and (b) Nyquist plots of the CNT/PEI/GOx catalysts measured under glucose concentrations of 0, 2, 4, 6, 8 and 10 mg·mL^{-1} at air state, while (c) and (d) are the CV curves and Nyquist plots of the catalysts measured under glucose concentrations of 0 and 10 mgmL^{-1} at N$_2$ state. Potential scan rate used was 100 mV·s^{-1}.
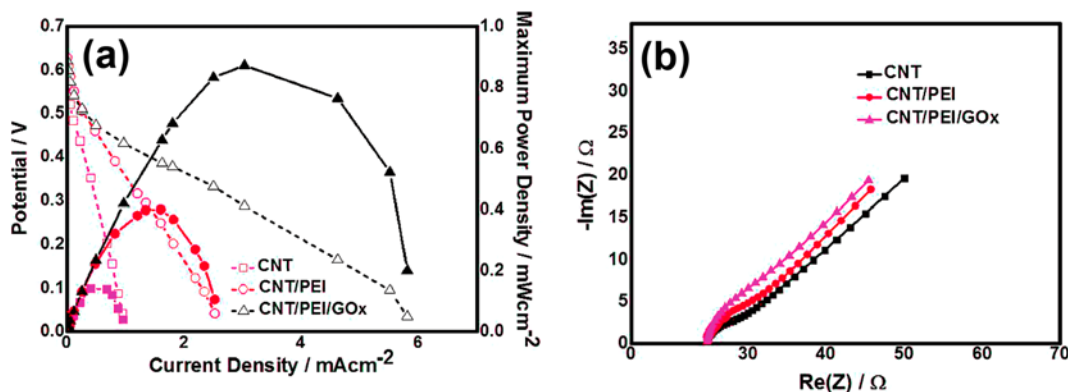

Fig. 7. Maximum Power Density (MPD) of (a) CNT, CNT/PEI, and CNT/PEI/GOx. While (b) their Nyquist plot. In the tests, aerated 0.2 M glucose solution was fed and circulated from an external bottle to the anode reservoir of EBC at a rate of 0.1 mL·min^{-1}, For cathodic reaction, 100 cc·min^{-1} O$_2$ (MPD test) or H$_2$ (EIS test) gas was fed.

as shown in Fig. 6(d). In brief, because of lack of mediator, electron transfer between the electrolyte and electrode including the enzymatic catalyst was not further activated. In turn, this result did not affect changes in the conductivity at the electrode, followed by in the R$_{ct}$.

4. Performance of GBFC Adopting CNT/PEI/GOx

To inspect the effect of CNT/PEI/GOx catalyst on EBC performance, it is important to investigate the performance of the EBCs using the CNT, CNT/PEI and CNT/PEI/GOx as anodic catalysts and the Pt/C as cathodic catalyst by measuring polarization curves; and the measuring result is represented in Fig. 7(a). For obtaining normalized result, the polarization curves were at least measured twice with two samples per case. According to Fig. 7(a), the maximum power density (MPD) of the EBC using the CNT/PEI/GOx was highest than that using the CNT and CNT/PEI (MPD of EBCs adopting CNT, CNT/PEI, and CNT/PEI/GOx was 0.14, 0.4,

and 0.87 mW·cm^{-2}). Such a pattern in MPD was similar to that in CV curves of Fig. 3(a). Namely, when the PEI was adopted, EBC MPD increased 185.7% from 0.14 to 0.4 mW·cm^{-2}, while when the GOx was further included, EBC MPD increased 118% from 0.4 to 0.87 mW·cm^{-2}. In Fig. 3(a), Nyquist plots of the EBCs that were the same structure to the Fig. 7(a) were also measured to determine R_{ct} and R_s (Fig. 7(b)). As a result, like other Nyquist plot data, R_ss of all the EBCs were similar (25.3-25.9 Ω), while R_{ct}s of the EBCs using the CNT, CNT/PEI and CNT/PEI/GOx were 9.2, 11.5, and 14.5 Ω, respectively. These phenomena are compatible with a pattern of the Nyquist plots shown in Fig. 3(b), so when the GOx and PEI were included as components consisting of the catalysts, R_{ct}s of the catalysts increased due to the nonconductive property of the GOx and PEI [22,31].

CONCLUSIONS

A new biocatalyst, CNT/PEI/GOx, was developed and CV pattern of the corresponding catalysts (CNT, CNT/PEI, and CNT/PEI/GOx catalysts) was examined and compared regarding their R_{ct}s that was attained by Nyquist plots using EIS. According to examination and comparison of the CVs and Nyquist plots, reactivity of FAD redox reaction measured by both CV and R_{ct} showed a close relationship. In addition, as parameters affecting the reactivity of FAD redox reaction, concentrations of GOx, glucose and phosphorous buffer solution, electrolyte pH and ambient condition were chosen and their effects were investigated by the CV curves and Nyquist plots.

In experimental evaluations, it was confirmed that the reactivity of FAD redox reaction was connected with R_{ct}, which means that the difference in reactivity of FAD redox reaction that occurred at the different catalysts can be simply predicted by examination of their R_{ct}s. As an example showing the relationship, the performance of the EBCs using the catalysts was considered. When their MPDs were examined, their trends were compatible with those in their R_{ct}s, proving that there was a close correlation between the CV curves and Nyquist plots regarding the reactivity of FAD redox reaction.

ACKNOWLEDGEMENT

REFERENCES

1. A. Zebda, S. Cosnier, J.-P. Alcaraz, M. Holzinger, A. Le Goff, C. Gondran, F. Boucher, F. Giroud, K. Gorgy, H. Lamraoui and P. Cinquin, *Sci. Rep.*, **3**, 1516 (2013).
2. A. Zebda, C. Gondran, A. Le Goff, M. Holzinger, P. Cinquin and S. Cosnier. *Nat. Commun.*, **2**, 370 (2011).
3. A. Zebda, L. Renaud, M. Cretin, C. Innocent, F. Pichot, R Ferrigno and S. Tingry. *J. Power Sources*, **193**, 602 (2009).
4. H. S. Choi, D. S. Kim, L. P. Thapa, S. J. Lee, S. B. Kim, J. Cho, C. Park and S. W. Kim, *Korean J. Chem. Eng.*, **33**, 3434 (2016).
5. R. A. Bohara, N. D. Thorat and S. H. Pawar, *Korean J. Chem. Eng.*, **33**, 216 (2016).
6. S. Cosnier, A. Le Goff and M. Holzinger, *Electrochem. Commun.*, **38**, 19 (2014).
7. S. C. Barton, J. Gallaway and P. Atanassov, *Chem. Rev.*, **104**, 4867 (2004).
8. K. Y. Kwon, J. Youn, J. H. Kim, Y. Park, C. Jeon, B. C. Kim, Y. Kwon, X. Zhao, P. Wang, B. I. Sang, J. Lee, H. G. Park, H. N. Chang, T. Hyeon, S. Ha, H. T. Jung and J. Kim, *Biosens Bioelectron.*, **26**, 655 (2010).
9. E. H. Yu, U. Krewer and K. Scott, *Energies.*, **3**, 1499 (2010).
10. Y. Chung, K. Hyun and Y. Kwon, *Nanoscale.*, **8**, 1161 (2016).
11. S. Han, G. S. Chae and J. S. Lee, *Korean J. Chem. Eng.*, **33**, 1799 (2016).
12. A. Kavitha and K. B. Yazhini, *Korean J. Chem. Eng.*, **33**, 1948 (2016).
13. K. Shimizu and M. Ishihara. *Biotechnol. Bioeng.*, **29**, 236 (1987).
14. Y. Wei, J. Xu, Q. Feng, M. Lin, H. Dong, W. Zhang and C. J. Wang, *Nanosci. Nanotechnol.*, **1**, 83 (2001).
15. K. Szymánska, J. Bryjak and A. B. Jarzębski, *Top. Catal.*, **52**, 1030 (2009).
16. R. Schoevaart, M. W. Wolbers, M. Golubovic, M. Ottens, A. P. G. Kieboom, F. van Rantwijk, L. A. M. van der Wielen and R. A. Sheldon, *Biotechnol. Bioeng.*, **87**, 754 (2004).
17. D. N. Tran and K. J. Balkus. *ACS Catal.*, **1**, 956 (2011).
18. I. Willner, A. Riklin, B. Shoham, D. Rivenzon and E. Katz. *Adv. Mater.*, **5**, 912 (1993).
19. I. Willner, V. Heleg-Shabtai, R. Blonder, E. Katz, G. Tao, A. F. Bückmann and A. Heller *J. Am. Chem. Soc.*, **118**, 10321 (1996).
20. I. Willner, E. Katz and B. Willner, *Electroanalysis*, **9**, 965 (1997).
21. M. Christwardana, Y. Chung and Y. Kwon, *Nanoscale*, **9**, 1993 (2017).
22. K. H. Hyun, S. W. Han, W. G. Koh and Y. Kwon, *J. Power Sources*, **286**, 197 (2015).
23. Inamuddin, Beenish, and Mu. Naushad, *Korean J. Chem. Eng.*, **33**, 120 (2016).
24. M. Wooten, S. Karra, M. Zhang and W. Gorski, *Anal. Chem.*, **86**, 752 (2014).
25. R. K. Shervedani, A. H. Mehrjardi and N. Zamiri, *Bioelectrochemistry*, **69**, 201 (2006).
26. P. Mulchandani, A. Mulchandani, I. Kaneva and W. Chen, *Biosens Bioelectron.*, **14**, 77 (1999).
27. R. Yuan, D. Tang, Y. Chai, X. Zhong, Y. Liu and J. Dai, *Langmuir*, **20**, 7240 (2004).
28. Y. Chung, Y. Ahn, M. Christwardana, H. Kim and Y. Kwon, *Nanoscale*, **8**, 9201 (2016).
29. M. Christwardana and Y. Kwon, *J. Power Sources*, **299**, 604 (2015).
30. Y. Ahn, K. S. Yoo, L. H. Kim and Y. Kwon, *Int. J. Hydrogen Energy*, **41**, 17548 (2016).
31. S. Duan, R. Yue and Y. Huang, *Talanta*, **160**, 607 (2016).
32. J. E. Fischer, H. Dai, A. Thess, R. Lee, N. M. Hanjani, D. L. Dehaas and R. E. Smalley, *Phys. Rev.*, **55**, R4921 (1997).
33. B. Marinho, M. Ghislandi, E. Tkalya, C. E. Koning and G. de With, *Powder Technol.*, **221**, 351 (2012).
34. G. Zou, M. Jain, H. Yang, Y. Zhang and D. Williams, Q. Jia, *Nanoscale*, **2**, 418 (2010).
35. S. Deng, G. Jian, J. Lei, Z. Hu and H. Ju, *Biosens Bioelectron.*, **25**, 373 (2009).

36. W.-C. Chen, T.-C. Wen, C.-C. Hu and A. Gopalan, *Electrochim. Acta*, **47**, 1305 (2002).

37. A. M. Johnson, D. R. Sadoway, M. J. Cima and R. Langer, *J. Electrochem. Soc.*, **152**, H6 (2005).

38. C. Prodan and C. Bot, *J. Phys. D: Appl. Phys.*, **42**, 175505 (2009).

39. J. Ji, M. Christwardana, Y. Chung and Y. Kwon, *Trans. Korean Hydrogen New Energy Soc.*, **27**, 526 (2016).

40. K. H. Hyun, S. W. Han, W. G. Koh and Y. Kwon, *Int. J. Hydrogen Energy*, **40**, 2199 (2015).

41. M. Christwardana, K. J. Kim and Y. Kwon, *Sci. Rep.*, **6**, 3012 (2016).

42. D. Ivnitski, B. Branch, P. Atanassov and C. Apblett. *Electrochem. Commun.*, **8**, 1204 (2006).

43. D. Ivnitski, K. Artyushkova, R. A. Rincon, P. Atanassov. H. R. Luckarift and G. R. Johnson, *Small.*, **4**, 357 (2008).

44. S. B. Bankar, M. V. Bule, R. S. Singhal and L. Ananthanarayan, *Biotechnol. Adv.*, **27**, 489 (2009).

45. C. Tlili, K. Reybier, A. Géloën, L. Ponsonnet, C. Martelet, H. B. Ouada, M. Lagarde and N. Jaffrezic-Renault, *Anal. Chem.*, **75**, 3340 (2003).